PHILOSOPHICAL TRANSACTIONS A

royalsocietypublishing.org/journal/rsta





Article submitted to journal

Subject Areas:

High energy density, atomic, plasma

Keywords:

average atom, non-LTE, opacity, density functional theory

Author for correspondence:

Stephanie B. Hansen e-mail: sbhanse@sandia.gov

Self-consistent and detailed opacities from a non-equilibrium average-atom model

S. B. Hansen¹

¹Pulsed Power Sciences Center, Sandia National Laboratories, Albuquerque, NM 87123

Modern density functional theory (DFT) is a powerful tool for accurately predicting self-consistent material properties such as equations of state, transport coefficients, and opacities in high energy density plasmas, but it is generally restricted to conditions of local thermodynamic equilibrium (LTE) and produces only averaged electronic states instead of detailed configurations. We propose a simple modification to the bound-state occupation factor of a DFT-based average-atom model that captures essential non-LTE effects in plasmas - including autoionization and dielectronic recombination - thus extending DFTbased models to new regimes. We then expand the self-consistent electronic orbitals of the non-LTE DFT-AA model to generate multi-configuration electronic structure and detailed opacity spectra.

1. Introduction

Understanding the properties and responses of matter at extreme conditions is a critical component of high energy density (HED) science, relevant to diverse plasma systems including stars, giant planets, and inertial confinement fusion (ICF) [1]. Simulations and diagnostics of these HED systems require wide-ranging and accurate data for equations of state, transport coefficients, and radiative properties such as emission and opacity spectra, which must be known over a wide range of conditions, from cold and warm dense matter in local thermodynamic equilibrium (LTE) to hot, small-scale, and highly transient non-LTE plasmas. Since benchmark HED experiments are difficult to perform [2], these properties are difficult to measure. They are also difficult to calculate, since models must capture a complex interplay of quantum, thermal, collective, configurational, and non-equilibrium effects.

© The Authors. Published by the Royal Society under the terms of the Creative Commons Attribution License http://creativecommons.org/licenses/by/4.0/, which permits unrestricted use, provided the original author and source are credited.

THE ROYAL SOCIETY PUBLISHING



Density functional theory (DFT) [3] offers a powerful predictive tool for HED. Multi-ion DFT codes like the Vienna Ab-initio Simulation Package (VASP) [4] track both the classical motion of multiple ions and the fully quantum dynamic response of electrons, predicting properties like melt temperatures, pressures, and conductivities with high accuracy when averaged over many ionic configurations. However, these multi-ion quantum codes are computationally expensive, especially at high temperatures and for many-electron atoms. DFT-based average-atom (AA) codes like Inferno [5] and Purgatorio [6] collapse the ionic configurations into a spherical average but offer fully quantum all-electron calculations that remain computationally efficient for arbitrarily high temperatures. Both of these DFT-based models predict averaged electronic structure, rather than detailed electronic configurations. And both are generally restricted to LTE, where ions, electrons, and photons all have equal temperatures and thermal energy distributions.

While LTE is a good approximation in long-lived systems like stellar interiors, it can be difficult to achieve and maintain in HED experiments driven by transient pulses of particles, photons, currents, implosions, or shocks. These drivers preferentially deposit energy into either electrons (e.g. optical or X-ray lasers) or ions (e.g. implosions and shocks), leading to a transient non-equilibrium between ion and electron temperatures. The associated material properties can still be accurately modeled using DFT-based models, however, as long as the electron distribution remains thermal.

Thermal equilibrium among electrons is enforced by detailed balance between upward and downward rates. At low temperatures (< 10eV) and high densities (near solid), collisional processes are extremely effective at thermalizing electron energy distributions. At higher temperatures, lower densities, and especially for high-Z materials in which spontaneous radiative decay rates are much larger than collisional excitation rates, recovering statistical equilibrium through detailed balance requires high radiation temperatures. But thermal radiation fields carry an enormous amount of energy: even the world's largest HED experimental facilities [1] cannot maintain Planckian radiation fields with temperatures T_r above several hundred eV. Thus, there is a large class of non-LTE HED laboratory plasmas with $T_r \ll T_e$ that cannot be modeled with standard DFT-based models.

High-temperature non-LTE plasmas are typically modeled with collisional-radiative (CR) codes [7–9], which solve sets of coupled rate equations among multiple electronic configurations. These multiconfiguration (MC) models can also provide detailed spectra that can be directly compared with experimental measurements. However, CR codes are typically based on isolatedion electronic structure and require *ad-hoc* corrections to account for dense plasma effects that can change both the electronic structure and the associated rates.

This work attempts to combine the strengths of DFT and CR models, describing an efficient and self-consistent model that can account for both non-LTE and dense plasma effects on plasma properties including detailed spectra suitable for comparison with experiment. In Section 2, we offer a simple modification of the occupation factors used in a DFT-based average-atom model (DFT-AA) that captures the effects of imbalances between collisional and radiative ionization and recombination rates in non-LTE plasmas with $T_r \neq T_e$. We also offer a new approach to incorporating dielectronic recombination and excitation-autoionization processes that further improves the non-LTE predictions. In Section 3, we use the self-consistent DFT-AA electronic states to generate multi-configuration electronic structure and spectra suitable for direct comparison with experiments. Section 4 concludes with a summary and discussion of future work, including possible extensions to multi-ion DFT models, improvements to the DFT-AA-MC model, and applications to transient plasmas.

2. Non-LTE average-atom model

Average-atom models distill the complexities of multiple ionic and electronic configurations into a single, averaged ion with spherical symmetry and non-integer electronic occupations. In this work, we follow previous implementations of fully quantum mechanical DFT-AA models

[5,6] that solve for self-consistent electronic orbitals and electron-ion potentials $V_{ei}(r)$ within a Wigner-Seitz sphere of radius $r_0 = (3/(4\pi n_i))^{1/3}$, with n_i the ion density. Our model solves the Schrödinger equation in a semi-relativistic potential with the Kohn-Sham local density approximation for exchange [3] and boundary condition $V_{ei}(r_0) = 0$. For a given potential, this yields (negative) bound-state orbital binding energies $\varepsilon_{n\ell}$ and both bound $P_{n\ell}(r)$ and continuum $P_{\varepsilon\ell}(r)$ radial electronic orbitals. Since the screened potential depends on the radial electron density distribution, which is a function of the electronic orbitals $P_a(r)$ and their occupation factors, calculations of potentials and orbitals must be iterated until they converge. At convergence, the orbitals self-consistently include dense plasma effects such as continuum lowering and pressure ionization.

In LTE, the electronic orbitals are populated according to the product of their statistical weights $g_\ell=2(2\ell+1)$ and Fermi-Dirac occupation factors $f(\varepsilon)=(1+e^{(\varepsilon-\mu)/T_e})^{-1}$, with the chemical potential μ variationally constrained to enforce neutrality within the ion sphere. The total electron charge density can be used to provide several plausible definitions for the average ionization Z^* [10]. Here, we count all positive-energy electrons as contributors to Z^* , integrating the product of $f(\varepsilon)$ and the quantum density of states over energy to obtain Z^* . The Fermi-Dirac occupation factors are foundational to all DFT-based methods, and, with few exceptions ([11–14]), LTE is a standard assumption for AA models.

LTE occupation factors like $f(\varepsilon)$ (and associated Boltzmann and Saha-Bolztmann statistics) are enforced through detailed balance among collisional and radiative upward and downward rates. When collisions alone do not enforce detailed balance, either because densities are small or spontaneous radiative decay rates are large, Planckian radiation fields with $T_r = T_e$ can enforce detailed balance among the radiative rates and recover LTE. When electron energy distributions or radiation fields are non-thermal, non-LTE solution methods such as collisional-radiative (CR) models are required to find state occupations. CR methods solve a set of coupled rate equations for integer-occupied electronic configurations to obtain either steady-state or time-dependent occupations [7] in non-LTE plasmas. Generalizing these CR methods for average atom models is not trivial, however, largely because of the complexity of the two-step dielectronic recombination and excitation-autoionization processes.

Our approach is based on the observation that, by construction, the detailed balance of collisional ionization and three-body recombination rates $R_{Z\to Z+1}^{cion}$ and $R_{Z+1\to Z}^{3rec}$ enforce LTE statistics [16,17] between the populations X^Z and X^{Z+1} of the ground configurations of adjacent charge states with equal statistical weights:

$$\frac{X^{Z+1}}{X^Z} = \frac{R_{Z \to Z+1}^{cion}}{R_{Z+1 \to Z}^{3rec}} = e^{(-\varepsilon_Z - \mu)/T_e}.$$
 (2.1)

Here, ε_Z is the (positive) ionization potential of the ion with charge Z. In the DFT-AA formalism, the ionization potential of a particular bound $n\ell$ electron is $\varepsilon_Z = |\varepsilon_{n\ell}| = -\varepsilon_{n\ell}$. We thus propose replacing the Fermi-Dirac occupation factor used to populate the $n\ell$ orbitals of the DFT-AA model as follows:

$$f^{\rm LTE}(\varepsilon_{n\ell}) = \frac{1}{1 + {\rm e}^{(\epsilon_{n\ell} - \mu)/T_e}} \to f^{\rm non-LTE}(\varepsilon_{n\ell}) = \frac{1}{1 + R_{n\ell}^{\rm ion}/R_{n\ell}^{\rm rec}} \tag{2.2}$$

with $R_{n\ell}^{\rm ion}$ and $R_{n\ell}^{\rm rec}$ the total ionization and recombination rates $per\ n\ell$ electron in the AA model. These total rates should include not only collisional ionization and three-body recombination, but also photoionization, radiative recombination (both spontaneous and stimulated), excitation-autoionization, and dielectronic recombination. This approach is closely related to Rozsnyai's one-level continuum approximation [13]. When $T_e = T_r$, Eq. 2 recovers the Fermi-Dirac occupation factor and LTE. When electron or photon distributions are nonthermal (as in beam-driven, photoionized or XFEL plasmas), additional ionization processes can decrease occupation factors for bound electrons and drive the plasma ionization to higher Z^* values. When $T_r \ll T_e$, the excess radiative recombination will tend to increase occupation factors for bound electrons, resulting in smaller Z^* values.

(a) Collisional ionization and photoionization

For collisional ionization, we use the simple Lotz prescription for the cross section per bound electron [18]:

$$\sigma^{\text{cion}} = 2Ry^2 \pi a_0^2 \frac{\ln(\varepsilon_i/|\varepsilon_{n\ell}|)}{\varepsilon_i|\varepsilon_{n\ell}|} = 3.3 \times 10^{-14} \frac{\ln(\varepsilon_i/|\varepsilon_{n\ell}|)}{\varepsilon_i|\varepsilon_{n\ell}|} \text{cm}^2$$
(2.3)

with Ry the Rydberg energy in eV, a_0 the Bohr radius in cm, ε_i the impact electron energy in eV, and $\varepsilon_{n\ell}$ the $n\ell$ state binding energy in eV. The collisional ionization rate is calculated by integrating this cross section over the electron energy distribution, and the three-body recombination rate is obtained from detailed balance.

For photoionization, we use the Kramers semiclassical cross section per bound electron [19]:

$$\sigma^{\text{pion}} = Ry\pi a_0^2 \frac{64\alpha}{3\sqrt{3}} \frac{|\varepsilon_{n\ell}|^2}{n\omega^3} = 1.1 \times 10^{-16} \frac{|\varepsilon_{n\ell}|^2}{n\omega^3} \text{cm}^2$$
(2.4)

with α the fine structure constant, n the principal quantum number of the ionizing state, and ω the incident photon energy in eV. The photoionization rate is calculated by integrating this cross section over the photon energy distribution, and the radiative recombination rate is found by integrating the associated radiative recombination cross section, $\sigma^{\rm rrec} = 1.1 \times 10^{-22} |\varepsilon_{n\ell}|/(n\varepsilon_i) {\rm cm}^2$, over the electron energy distribution.

For non-degenerate (Maxwellian) electron distributions and $T_r = 0$, the associated rates are:

$$R^{\text{cion}} = 2.2 \times 10^{-6} n_e \frac{\chi(\beta) e^{-\beta}}{|\varepsilon_{n\ell}| T_e^{1/2}} \text{ s}^{-1}$$
 (2.5)

$$R^{3\text{rec}} = 3.6 \times 10^{-28} n_e^2 \frac{\chi(\beta)}{|\varepsilon_{n\ell}| T_e^2} \,\text{s}^{-1}$$
 (2.6)

$$R^{\text{rrec}} = 7.0 \times 10^{-15} n_e \frac{\chi(\beta) |\varepsilon_{n\ell}|^2}{n T_e^{3/2}} \text{ s}^{-1}$$
 (2.7)

with $\beta = |\varepsilon_{n\ell}|/T_e$ and $\chi(\beta) = \ln[1 + (0.562 + 1.4\beta)/(\beta + 1.4\beta^2)]$, T_e in eV, and n_e in cm⁻³. When electrons are partially or fully degenerate, integrations over electron energy distributions should be done numerically and include Pauli blocking factors [20].

These simple expressions provide a reasonable first estimate of non-LTE effects in any DFT-based model from the straightforward substitution of the Fermi-Dirac occupation factor given in Eq. 2. The resulting Z^* for $0.01\,\mathrm{g/cm^3}$ krypton with $T_r=0$ are given by the dark yellow line in Fig. 1. At high temperatures, the imbalance between R^{rrec} and $R^{\mathrm{pion}}=0$ leads to a dramatic difference in Z^* from the LTE calculation. The non-LTE DFT-AA model agrees relatively well with both a screened hydrogenic CR model [8] that uses the same rate approximations and a hybrid-structure model [9] that uses rate coefficients calculated from FAC [21], when those CR models exclude autoionization and dielectronic recombination.

(b) Autoionization and dielectronic recombination

Previous efforts to modify quantum average-atom models to account for non-LTE effects [13,14] have been complicated by the difficulty of accounting for the two-electron, two-step processes of excitation-autoionization (EA) and dielectronic recombination (DR). Both of these processes are mediated by Auger decay (autoionization) rates, A^a , which describe the decay of inner-shell or multiply excited states in an ion with charge Z whose excitation energy is larger than its ground-state ionization potential ε_Z . In the Auger decay process, one excited electron (i) in the ion with charge Z decays to the ground state (f) of the ion with charge Z+1, giving its decay energy to the other excited electron (j), which is ejected into a continuum state c. Dielectronic capture is the reverse process, in which an electron captured from the continuum excites a second electron in the capturing ion. Autoionizing states can be generated by either dielectric capture from the

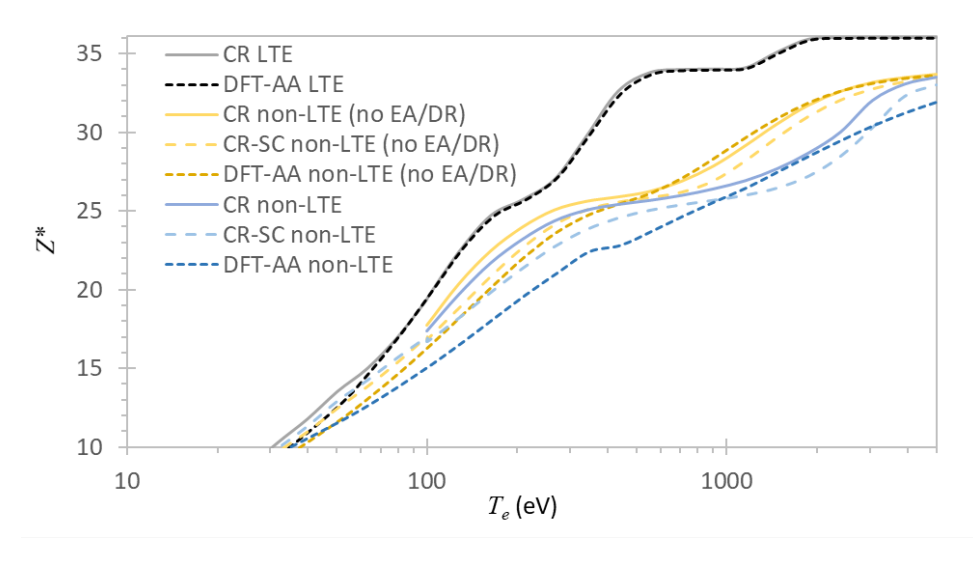


Figure 1. Average ionization Z^* for 0.01 g/cm³ Kr from the DFT-AA model described in the text for LTE $(T_r = T_e)$ and non-LTE $(T_r = 0)$ conditions, compared to two collisional-radiative models: a screened-hydrogenic super-configuration model (CR-SC) [8] and a more detailed hybrid-structure model (CR) [9]. For all models, the non-LTE Z^* are given with (blue) and without (yellow) excitation-autoionization and dielectronic recombination.

Z+1 or multiple excitation from Z, and they can decay by either (radiationless) autoionization into Z+1 or radiative decay into a non-autoionizing state in Z.

These processes can be difficult enough to model in a CR formalism with integer-occupied configurations that explicitly track electron transitions and configuration energies, and many CR models simplify the calculation by invoking approximations based on one-electron oscillator strengths [22]. The two-step processes are even more challenging in average-atom models, whose one-electron orbitals and non-integer shell occupations preclude explicit tracking of multiply excited configurations. Quantum DFT-AA models, however, have the advantage of providing self-consistent radial wavefunctions, $P_{n\ell}$ for bound states and $P_{\varepsilon\ell}$ for continuum states, which enable a perturbation-theory calculation of A^a .

Following [23], we directly compute Auger decay rates from the time uncertainty (lifetime) of interacting DFT-AA states i, j, f, and c:

$$A_{ijf}^{a} = \frac{2\pi}{\hbar} |R^{k}(ij, fc)|^{2} = 2.6 \times 10^{17} |R^{k}(ij, fc)|^{2} \text{ s}^{-1},$$
 (2.8)

with $|R^k(ij, fc)|^2$ is in Hartree atomic units and radial integrals

$$R^{k}(ij, fc) = \int_{0}^{r_{0}} \left\{ \frac{1}{r_{2}^{k+1}} \int_{0}^{r_{2}} r_{1}^{k} P_{i}^{*} P_{f} dr_{1} + r_{2}^{k} \int_{r_{2}}^{r_{0}} \frac{1}{r_{1}^{k+1}} P_{i}^{*} P_{f} dr_{1} \right\} P_{j}^{*} P_{c} dr_{2}$$
 (2.9)

Here, the states i and j are the active DFT-AA orbitals of an autoionizing state (e.g. 2p and 2s in the doubly excited 2s2p configuration of an He-like ion), f is the DFT-AA orbital of the final bound state after autotionization (e.g. H-like 1s), and c is the continuum state with energy $\varepsilon_c = \varepsilon_i + \varepsilon_j - \varepsilon_f$. We enforce dipole selection rules and conservation of angular momentum: $|\ell_i - \ell_f| = 1$ and $\ell_c = \ell_j + \ell_i - \ell_f$.

To estimate the two-step EA and DR processes, we must also calculate radiative decay rates:

$$A_{if}^{\mathbf{r}} = \frac{\alpha^3 Ry}{\hbar} \left(\frac{\varepsilon_i - \varepsilon_f}{Ry}\right)^2 f_{fi}^{\text{osc}} = 4.3 \times 10^7 (\varepsilon_i - \varepsilon_f)^2 f_{fi}^{\text{osc}} \,\text{s}^{-1}$$
 (2.10)

with dipole oscillator strengths

$$f_{fi}^{\text{osc}} = \frac{1}{3} \frac{(\varepsilon_i - \varepsilon_f)}{Ry} \left| \int_0^{r_0} P_i^* r P_f dr \right|^2$$
 (2.11)

Unlike the approximate collisional ionization and photoionization rates given above, these quantum evaluations significantly increase the runtime of the DFT-AA convergence loop. Thus, for each $n\ell$ state f, we restrict the present calculations to include only EA and DR processes associated with the dominant dipole transition $f \to i = n\ell \to (n+1)(\ell+1)$. Then, for every bound electron state j, we calculate total Auger rates $A_f^a = A_{ijf}^a + A_{jif}^a$ and total radiative decay rates $A_f^{\mathbf{r}} = A_{if}^{\mathbf{r}} + A_{jf}^{\mathbf{r}}$ (but if i = j, we do not double the rates).

To approximate the two-step EA process from each state f, we estimate the double collisional excitation rate R_{fi+fj}^{2cx} as a product of single excitation rates and an average excited state lifetime, $R_{f_i}^{ex}R_{f_i}^{ex}/(A_f^r/2)$. Assuming Mewe cross sections and a Maxwellian electron energy distribution, the single-excitation collision rates are:

$$R_{fk}^{\text{cx}} = 1.6 \times 10^{-5} n_e f_{fk}^{\text{osc}} \frac{[0.15 + 0.28\chi(\beta)]e^{-\beta}}{\Delta \varepsilon_{jk} T_e^{1/2}} \text{ s}^{-1},$$
 (2.12)

with $\Delta \varepsilon_{jk} = \varepsilon_k - \varepsilon_f$ and $\beta = \Delta \varepsilon_{jk}/T_e$. To account for the possibility that the doubly excited state can radiatively stabilize rather than complete the EA process, we multiply the double excitation rate $R_{fi+f}^{2\alpha}$ of each j by its value of the branching ratio $A_f^a/(A_f^a+A_f^r)$ and find the total effective ionization rate per electron in state f by summing over the contributions from all j. This ionization rate is then added to the total $R_{n\ell}^{\text{ion}}$ of Eq. 2.

Similarly, to approximate the two-step DR process into each state f, we again assume a Maxwellian distribution electron energy distribution and estimate a dielectronic capture rate for each j using its associated A_f^a value:

$$R_f^{\text{dc}} = 1.66 \times 10^{-22} n_e A_f^{\text{a}} \frac{e^{-\varepsilon_c/T_e}}{T_e^{3/2}} \text{ s}^{-1},$$
 (2.13)

The total DR rate into state f is then the sum over j of $R_f^{\text{dc}}A_f^{\text{r}}/(A_f^{\text{a}}+A_f^{\text{r}})$, and this effective recombination rate is added to the total $R_{n\ell}^{\text{rec}}$ of Eq. 2.

Incorporating these additional ionization and recombination terms into the non-LTE occupation factor used in the self-consistent DFT-AA model results in even lower ionization values than using only collisional and radiative processes, as shown by the dark blue lines in Fig 1. This trend follows the results of CR models that include explicit calculations of excitation, radiative decay, dielectronic capture, and autoionization among a large set of integer-occupied electronic configurations. While including EA and DR processes also tends to increase the disagreement among non-LTE models [7], the present approach offers a relatively good starting point for a multi-configuration expansion of the AA model - and it provides self-consistent, fully quantum electronic orbitals and screening that can be used to inform constitutive and response properties.

3. Non-LTE opacities

Opacities in HED plasmas control the flow of radiation and mediate energy exchange between plasma and atomic electrons. In careful benchmark experiments [2], detailed opacity measurements offer a rigorous test of atomic models. In this section, we describe two approaches to generating opacities from our non-LTE DFT-AA model: a Kubo-Greenwood approach that uses the self-consistent orbitals from the AA model, and a multiconfiguration (MC) approach that uses the AA orbitals as a basis set for energy integrals that are Taylor-expanded to provide detailed integer-occupied electronic configurations and opacity spectra.

(a) Kubo-Greenwood

The Kubo-Greenwood (KG) approach offers a baseline for investigations into self-consistent frequency-dependent (dynamic) response functions. For the DFT-AA model, [24] have derived a relatively straightforward expression for the optical conductivity based on dipole cross sections between every pair of quantum AA orbitals. The KG dynamic conductivity includes bound-bound, bound-free, and free-free contributions, and is given by:

$$\sigma_r(\omega) = \frac{2\pi n_i}{\omega} \int d\varepsilon [f(\varepsilon_a) - f(\varepsilon_{a'})] \int d^3q_a \int d^3q_{a'} |\langle P_a | \mathbf{v} | P_{a'} \rangle|^2 \delta(\varepsilon_a - \varepsilon_{a'} - \omega)$$
 (3.1)

The imaginary part of the KG dynamic conductivity (or any other dynamic response function) can be calculated using the Kramers-Kronig dispersion relation: $\sigma_i(\omega) = -\frac{2}{\pi} P \int d\omega' \sigma_r(\omega') \omega/(\omega'^2 - \omega^2)$, where P is the principal value (avoiding the poles). The complex dynamic conductivity can then be used to generate a wide range of dynamic material properties including the dielectric function $\epsilon(\omega)$, the index of refraction $\eta(\omega)$, and the absorption opacity $\kappa(\omega)$ [25,26]:

$$\epsilon_r(\omega) = 1 - \frac{4\pi}{\omega} \sigma_i(\omega)$$
 (3.2)

$$\epsilon_i(\omega) = \frac{4\pi}{\omega} \sigma_r(\omega) \tag{3.3}$$

$$\eta(\omega) = \frac{1}{2^{1/2}} [|\epsilon(\omega)| + \epsilon_r(\omega)]^{1/2}$$
(3.4)

$$\kappa(\omega) = \frac{4\pi}{\eta(\omega)c}\sigma(\omega). \tag{3.5}$$

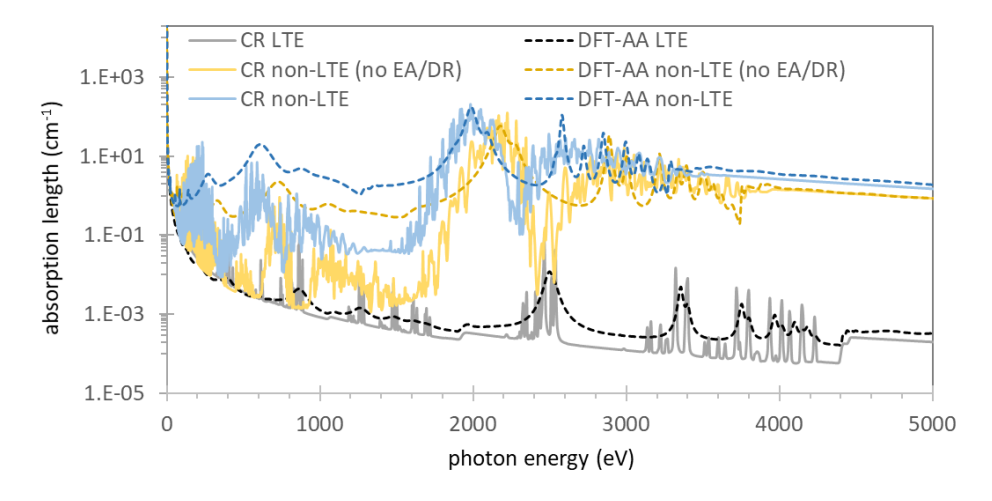


Figure 2. Absorption coefficients for $T_e=2~{\rm keV},~0.01~{\rm g/cm^3}~{\rm krypton}$ from Kubo-Greenwood calculations based on self-consistent LTE and non-LTE DFT-AA orbitals (dashed lines) compared against absorption from a hybrid-structure collisional-radiative model (solid lines). Both models show profound non-LTE effects.

Figure 2 shows Kubo-Greenwood absorption coefficients based on the self-consistent non-LTE DFT-AA orbitals and compares them against the results of the hybrid-structure CR model SCRAM [9]. The one-electron DFT-AA-KG transitions are given broad Lorentzian line profiles with arbitrary line widths of 50 - 100 eV, while the detailed model has an imposed spectral resolution of $E/\Delta E = 500$. Both models show profound non-LTE effects, including order-of-magnitude differences in bound-free absorption and large shifts in the energies of bound-bound absorption

envelopes. Although the DFT-AA model reproduces the trends of the CR model, it gives a much simpler bound-bound spectrum in which every one-electron transition is represented as a single line (e.g. 2s-3p), while the CR model is composed of thousands of spin-orbit-split $(2s_{1/2}[n\ell_j...]-3p_{1/2}[n\ell_j...]$ and $2s_{1/2}[n\ell_j...]-3p_{3/2}[n\ell_j...]$) and fine-structure transitions from a large number of ions and configurations with spectators $[n\ell_j...]$. The DFT-AA-KG spectrum also significantly overestimates M- and N-shell absorption, since our non-LTE treatment does not account for the imbalance between collisional excitation and radiative decay within the average atom.

(b) Multiconfiguration DFT-AA

While the non-LTE DFT-AA model presented so far gives a reasonable estimate for Z^* , it does not provide the detailed multiconfiguration (MC) electronic structure necessary for either a full CR rate matrix calculation or generation of detailed spectra. However, its self-consistent orbitals, which natively include plasma and density effects, offer a promising basis set that can be used with standard atomic physics methods [31] to generate detailed electronic configurations.

To systematically move from the AA orbitals to detailed MC electronic structure, we first enumerate real integer-occupied configurations about the average configuration. Starting with the integer-occupied ground configuration of an ion with the integer charge closest to \mathbb{Z}^* , we excite one electron from each occupied bound orbital into all orbitals with vacancies. This gives us a set of singly excited configurations, including inner-shell excitations. From each of these new configurations, we repeat the systematic excitation of electrons from occupied states into states with vacancies, avoiding duplicate configurations, to obtain a set of doubly excited states. This process can be iterated as often as desired, although the combinatorics can quickly lead to an intractable number of configurations (see [7]) so we here limit this expansion to triply excited states.

We then calculate the energies of each of those configurations using stored quantities calculated from the DFT-AA orbitals $P_{n\ell}(r)$. Following [30,31], we set the configuration-average binding energy of each $i=n\ell$ electron in each $[(n\ell)^N...]$ configuration to be $E^i=E^i_k+E^i_{nuc}+\sum_{j\neq i}E^{ij}$, the sum of its kinetic energy, its nuclear interaction energy, and its interaction energies with all other electrons in its configuration. The kinetic energies are:

$$E_k^i = \frac{1}{2} \int_0^{R_{WS}} P_i^* \left[-\frac{d^2}{dr} + \frac{\ell_i(\ell_i + 1)}{r^2} \right] P_i dr, \tag{3.6}$$

the electron-nuclear potential energies are:

$$E_{nuc}^{i} = \int_{0}^{R_{WS}} (-Z_{nuc}/r)|P_{i}|^{2} dr, \qquad (3.7)$$

and the interaction potential energies E^{ij} are given in terms of Slater integrals $F^k(ij) = R^k(ij,ij)$ and $G^k(ij) = R^k(ij,ji)$, with the radial integrals $R^k(ij,ba)$ given in Eq. (2.9), with

$$E^{ij} = F^{0}(ij) - \frac{1}{2} \sum_{k} \begin{pmatrix} \ell_{i} & k & \ell_{j} \\ 0 & 0 & 0 \end{pmatrix}^{2} G^{k}(ij)$$
 (3.8)

The configuration-average total binding energy of each N-electron configuration is $E_c = \sum_i (E_k^i + E_{nuc}^i + \frac{1}{2} \sum_{j \neq i} E^{ij})$. Note that since we restrict the integrals to the ion sphere, we capture the effects of pressure ionization as states dissolve into the continuum. Including quasibound (resonant) continuum states [27] ensures we capture orbitals that may be bound in one ion or configuration and unbound in another.

A significant deficiency of this first multiconfiguration model is that it does does not account for orbital relaxation, that is, how the orbital wavefunctions (and therefore Slater integrals, E_k^i , E_{nuc}^i , E^i_j , E^i , and E_c) change in response to changes in the configurations. This effect can be included by re-optimizing the self-consistent orbitals for each configuration (e.g. [32])

and recomputing the energies and Slater integrals for each. But this becomes computationally daunting for complex ions with many active electrons that may have many thousands of configurations. Instead, we modify the approach of [28]: after convergence is achieved in the DFT-AA model, we systematically move $\Delta N \approx 0.2$ electrons from each significantly occupied $(N_k = o(n_k \ell_k) > 1)$ bound orbital k into the continuum, re-converge the self-consistent field equations on that depleted AA configuration and supplemented continuum, recompute new Slater integrals and energies $a_i = E_k^i + E_{nuc}^i$ and $b_{ij} = E^{ij}$, and then define coefficients for a Taylor expansion of the energies under changes Δo_k in each orbital:

$$a'(ik) = \frac{(a_i^{AA} - a_i^{AA - \Delta o_k})}{\Delta o_k}$$
(3.9)

$$b'(ijk) = \frac{(b_{ij}^{AA} - b_{ij}^{AA - \Delta o_k})}{\Delta o_k}$$
(3.10)

This requires only a handful of re-optimizations that do not require particularly stringent convergence and allows us to generate reasonably accurate E_c for any configuration using $a_i = a_i^{AA} + \frac{1}{2} \sum_k a'(ik) \Delta N_k$ and $b_{ij} = b_{ij}^{AA} + \frac{1}{2} \sum_{j,k} b'(ijk) \Delta N_k$. We have tested the accuracy of the expansion by verifying that the predicted E_c for a given integer-occupied configuration changes by less than 0.1% even when it is several ionization stages or excitations removed from the reference DFT-AA configuration. Including orbital relaxation in this way is extremely efficient and gives transition energies that are slightly more accurate than those derived using the intermediate coupling approach described in [29].

To include the effects of the plasma electrons on the configuration energies [30], we perform one last re-optimization of the average-atom orbitals that retains the converged AA bound-state occupations but excludes all continuum electrons from the Wigner-Seitz sphere. For each orbital i, this gives an isolated-ion binding energy of $\varepsilon_{n\ell}^0$ and a change in energy due to plasma electrons of $\Delta E_p^i = \varepsilon_{n\ell}^{\rm AA} - \varepsilon_{n\ell}^0$. Adding $\sum_i E_p^i$ to each configuration energy E_c gives a reasonable estimate for plasma density effects such as continuum lowering.

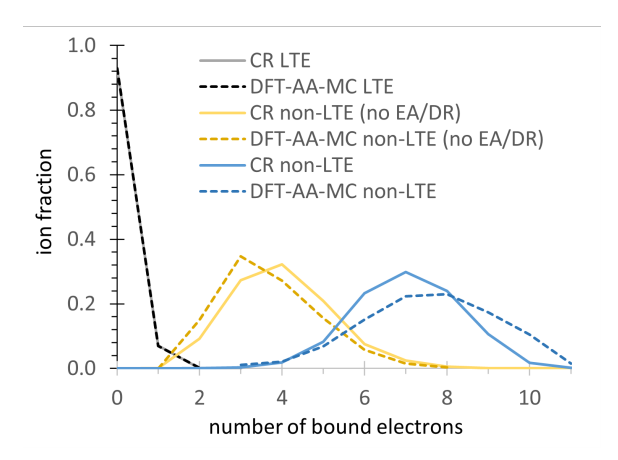


Figure 3. Charge state distributions for 0.01 g/cm 3 Kr at $T_e=2{\rm keV}$ from the DFT-AA-MC model described in the text (dashed lines) compared to a hybrid-structure CR model (solid lines).

To compute detailed spectra, we need not only the configuration energies but their occupations. We obtain ground-state occupations X_0 for each ion using factors derived from Eq. 2. Within each ion, we then assign excited-state occupations using Boltzmann factors: $X_c = X_0 \frac{g_c}{q_0} \exp[-|E_c - E_0|/T_{eff}]$ with an effective temperature derived from a two-level CR model

$$T_{eff} = \frac{-|E_c - E_0|}{\ln \frac{R^{ex}}{R^{dex}}}. (3.11)$$

Here, R^{ex} is the total collisional and photoexcitation rate from the ground to the excited configuration and R^{dex} is the total collisional, spontaneous, and stimulated decay rate. This yields not only the average ionization Z^* but also charge state distributions, as illustrated in Fig. 3. We then calculate the dipole matrix elements among just the DFT-AA orbitals to obtain oscillator strengths for each $n\ell \to n'\ell'$ transition, and assign radiative decay rates among configurations with occupation and vacancy factors as we would for a simple screened hydrogenic model [8].

Finally, we include relativistic effects in the spectrum by returning to the reference DFT-AA orbitals and computing the spin-orbit interaction:

$$E_{so}^{i} = \frac{\alpha^{2}}{2} \int_{0}^{R_{WS}} \frac{\partial V(r)}{\partial r} |P_{i}|^{2} dr$$
(3.12)

for states with $\ell>0$, which leads to splitting of the transitions into $j=\ell-\frac{1}{2}$ and $j=\ell+\frac{1}{2}$ components. Before computing the detailed spectra, we statistically weight the occupations and oscillator strengths of each of these components to preserve the total strength of the non-relativistic transitions. Here we also include correlation effects following Cowan. Together, the orbital relaxation, spin-orbit, and correlation modifications to the DFT-AA-MC model provide transition energies that have good agreement with detailed CR models like SCRAM [9] and experimental transition energies [2]. The results for krypton are given in fig. 4, where the DFT-AA-MC model reproduces not only the profound non-LTE effects seen in the detailed SCRAM CR model but also gives good agreement in line positions and significantly improves the DFT-AA-KG model's overprediction of M-and N-shell absorption.

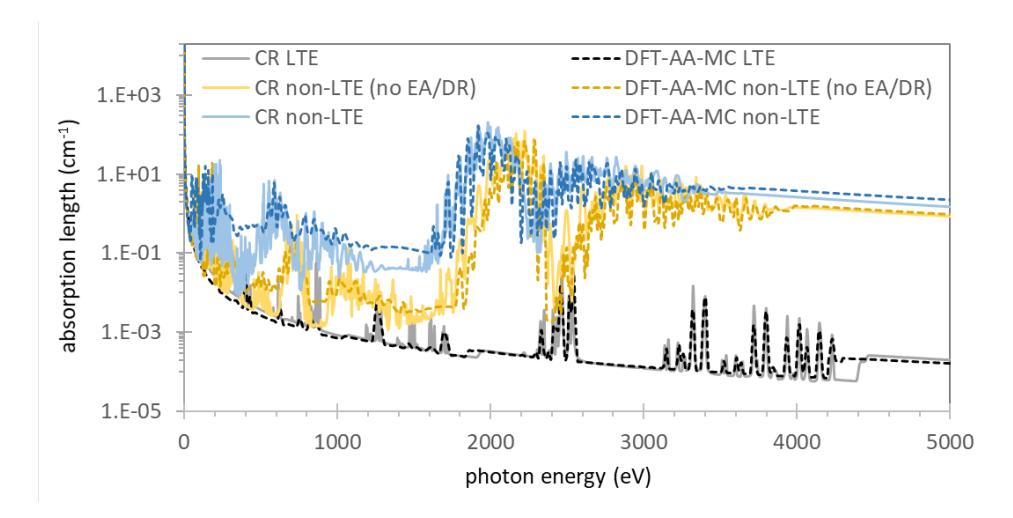


Figure 4. Absorption coefficients for $T_e=2\,$ keV, 0.01 g/cm 3 krypton from the DFT-AA-MC model (dashed lines) compared to a hybrid-structure CR model (solid lines).

4. Conclusion

We have presented an approach to generating non-LTE Z^* , charge state distributions, and detailed, multiconfiguration emission and opacity spectra based on the self-consistent electronic orbitals of a DFT-based average atom model. Our proposed simple modification to the Fermi-Dirac occupation factor approximately accounts for the imbalance in collisional and radiative

ionization and recombination in non-LTE plasmas with analytical rates that could be incorporated into any DFT-based model – including multi-ion DFT-MD. Extending the occupation factor to account for excitation-autoionization and dielectronic recombination based on the self-consistent quantum orbitals from DFT models offers a further refinement of the self-consistent Z^* . We have then used the non-LTE DFT-AA orbitals as a self-consistent basis set for multiconfiguration atomic structure, which, along with approximate effective temperatures allows us to obtain non-LTE level populations, charge state distributions, and detailed spectra.

This work significantly expands the useful range of DFT-AA models to non-LTE plasmas with $T_e \neq T_r$ and extends their predictive power to the generation of detailed spectra suitable for direct comparison with experiments. Other constitutive and response properties, such as pressures, internal energies, and conductivities, can also be derived from the self-consistent orbitals of the non-LTE DFT-AA model, which will natively include dense plasma effects such as continuum lowering (see [30]). This reduces the need for external models and ad-hoc approximations for dense plasma effects and will help ensure internal consistency among calculations of a wide variety of material properties.

The non-LTE DFT-AA model could be improved by explicitly accounting for the imbalance between collisional excitation and radiative decay rates within the DFT-AA model and by replacing the effective temperature approach in the DFT-AA-MC model with a full collisional-radiative solver. The self-consistency could be enhanced by recomputing the DFT-AA orbitals using fixed occupations obtained from the CR solution (see [15]. The detailed spectra could be improved with the inclusion of configuration interaction effects and more sophisticated line broadening. Possible extensions to the non-LTE DFT-AA model could include explicit time dependence to account for transient ionization and energy partitioning of the continuum electron distribution to explicitly track non-thermal free-electron distributions (e.g. populations of high-energy Auger or photoionized electrons in XFEL experiments) and their self-consistent effects on the average electronic structure. These modifications, which can be enormously expensive in traditional CR models, would be much more tractable in the AA model.

Acknowledgements. SH is grateful for conversations over many years with Brian Wilson, Charles Starrett, and Walter Johnson for contributions to the DFT-AA model, to Thomas Gomez for a correction in an early draft, and to the anonymous referees for their helpful comments. This work was supported by Sandia National Laboratories' Laboratory Directed Research and Development program under project 218456. Sandia National Laboratories is a multimission laboratory managed and operated by National Technology Engineering Solutions of Sandia, LLC, a wholly owned subsidiary of Honeywell International Inc., for the U.S. Department of Energy's National Nuclear Security Administration under contract DE-NA0003525. This paper describes objective technical results and analysis. Any subjective views or opinions that might be expressed in the paper do not necessarily represent the views of the U.S. Department of Energy or the United States Government.

References

- 1. Zylstra AB *et al.*, 2021. Record Energetics for an Inertial Fusion Implosion at NIF *Phys. Rev. Lett.* 126, 025001.
- 2. Bailey JE *et al.*, 2015. A higher-than-predicted measurement of iron opacity at solar interior temperatures, *Nature* **517**, 56–59.
- 3. Kohn, W and Sham LJ 1965. Self-Consistent Equations Including Exchange and Correlation Effects *Phys. Rev* **140**, A1133–A1138.
- 4. Kresse G and Furthmüller J, 1996. Efficient iterative schemes for ab initio total-energy calculations using a plane-wave basis set *Phys. Rev. B* **54**, 11169.
- 5. Liberman DA 1979. Self-consistent field model for condensed matter Phys. Rev. B 20, 4981–4989.
- 6. Wilson B, Sonnad V, Sterne P, and Isaacs W, 2006. Purgatorio: a new implementation of the Inferno algorithm, *J. Quant. Spectroscopy and Radiative Transfer* **99**, 658-679.
- 7. Ralchencko Yu, 2016. Modern Methods in Collisional Radiative modeling of Plasmas. Springer International.

- 8. Scott HA and Hansen SB, 2010. Advances in NLTE modeling for integrated simulations, *High Energy Density Physics* **6** 39-47.
- 9. Hansen SB, Bauche J, Bauche-Arnoult C, and Gu MF, 2007. Hybrid atomic models for spectroscopic plasma diagnostics, *High Energy Density Physics* **3**, 109–114.
- Murillo MS Weisheit J Hansen SB and DHarma-Wardana MWC, 2013. Partial ionization in dense plasmas: Comparisons among average-atom density functional models, *Phys. Rev. E* 87, 063113.
- 11. Lokke WA and Grassberger WH, 1977. XSNQ-U: a non-LTE emission and absorption coefficient subroutine, UCRL-52276.
- 12. Wilson BG and Albritton JR, 2000. NLTE ionization and energy balance in high-Z laser-plasmas including two-electron transitions, *J. Quant. Spectrosc. Radiat.Transfer* **65**, 1–13.
- 13. Rozsnyai BF, 1997. Collisional-radiative average-atom model for hot plasmas, *Phys. Rev. E*, **55**, 7507–7521.
- 14. Faussurier G, Blancard C and Berthier E, 2001. Nonlocal thermodynamic equilibrium self-consistent average-atom model for plasma physics, *Phys. Rev. E* **63**, 026401.
- 15. Faussurier G, Blancard C and Cosse P, 2014. Coupling of an average-atom model with a collisional-radiative equilibrium model, *Physics of Plasmas* **21**, 112707.
- 16. Cox AN, Stewart JN and Lilers DD, 1965. Effects of Bound-Bound Absorption on Stellar Opacities., *The Astrophysical Journal Supplement* 11, 1.
- 17. Luo G, 1994. The equation of state in the chemical picture: A grand canonical approach, *Astronomy and Astrophysics*, **281**, 460–464.
- 18. Lotz, W 1967. An empirical formula for the electron-impact ionization cross-section, *Zeitschrift für Physik* **206**,205–211.
- 19. Kramers HA, 1923. On the theory of X-ray absorption and of the continuous X-ray spectrum, *Philos. Mag.* **46**, 836–871.
- 20. Tallents GJ, 2016. Free electron degeneracy effects on collisional excitation, ionization, deexcitation and three-body recombination, *High Energy Density Physics* **20**, 9–16.
- 21. Gu MF, 2008. The flexible atomic code, Canadian Journal of Physics 86, 675-689.
- 22. Burgess A, 1965. General Formula for the Estimation of Dielectronic Recombination Co-Efficients in Low-Density Plasmas, *Astrophysical Journal* **141**, 1588–1590.
- 23. Cowan RD and Mann JR, 1979. Contribution of Autoionization to total ionization rates, *The Astrophysical Journal* 232, 940-947
- 24. Johnson WR, Guet C, and Bertsch GF, 2006. Optical properties of plasmas based on an averageatom model, *Journal of Quantitative Spectroscopy and Radiative Transfer* **99**, 327-340.
- 25. Mazevet S, Desjarlais MP, Collins LA Kress JD and Magee NH, 2005. Simulations of the optical properties of warm dense aluminum, *Phys. Rev. E* **71**, 016409.
- 26. Faussurier G, Blancard C. and Cossé P, 2015. Refractive index in warm and hot dense matter, *Phys. Rev. E* **91**, 053102.
- 27. Baczewski AD, Hentschel TW, Kononov A, and Hansen SB, 2021. Predictions of bound-bound transition signatures in x-ray Thomson scattering, doi = 10.48550/ARXIV.2109.09576
- 28. Wilson BG, 1993. Evaluating Orbital Occupation Number Correlations in High-Temperature Plasmas, J. Quant. Spectrosc. Radiat. Transfer 49, 241-258.
- 29. Goldberg A, Rozsnyai BF, and Thompson P, 1986 Intermediate-coupling calculation of atomic spectra from hot plasmas *Phys. Rev. A* **34**, 421–427.
- 30. Faussurier G and Blancard C, 2018. Density effects on electronic configurations in dense plasmas, *Phys. Rev. E* **97**, 023206.
- 31. Cowan RD, 1981. *The Theory of Atomic Structure and Spectra*. Berkeley, CA: University of California Press.
- 32. Gill NM, Fontes CJ, Starrett CE, 2023. A superconfiguration calculation of opacity with consistent bound and continuum electron treatments using Green's functions, *J. Phys. B* **56**, 015001.
- 33. Hansen SB, Baczewski AD, Gomez T, Hentschel TW, Jennings CA, Kononov A, Nagayama T, Adler K, Cangi A, Cochrane C, Robinson B, and Schleife A, 2022. Improving Predictive Capability in REHEDS Simulations with Fast, Accurate, and Consistent Non-Equilibrium Material Properties, SAND2022-13455.
- 34. , Hansen SB, Fournier KB, Bauche-Arnoult C, Bauche J, and Peyrusse O, 2006. A comparison of detailed level and superconfiguration models of neon, *J. Quantitative Spect. and Rad. Transf.* **99**, 272-282.